ARTICLE

doi:10.1038/nature11044

In vivo reprogramming of murine cardiac fibroblasts into induced cardiomyocytes

Li Qian[1,2,3], Yu Huang[1,2,3], C. Ian Spencer[1,2,3], Amy Foley[1,2,3], Vasanth Vedantham[1,4,5], Lei Liu[1,2,3], Simon J. Conway[6], Ji-dong Fu[1,2,3] & Deepak Srivastava[1,2,3]

The reprogramming of adult cells into pluripotent cells or directly into alternative adult cell types holds great promise for regenerative medicine. We reported previously that cardiac fibroblasts, which represent 50% of the cells in the mammalian heart, can be directly reprogrammed to adult cardiomyocyte-like cells *in vitro* by the addition of Gata4, Mef2c and Tbx5 (GMT). Here we use genetic lineage tracing to show that resident non-myocytes in the murine heart can be reprogrammed into cardiomyocyte-like cells *in vivo* by local delivery of GMT after coronary ligation. Induced cardiomyocytes became binucleate, assembled sarcomeres and had cardiomyocyte-like gene expression. Analysis of single cells revealed ventricular cardiomyocyte-like action potentials, beating upon electrical stimulation, and evidence of electrical coupling. *In vivo* delivery of GMT decreased infarct size and modestly attenuated cardiac dysfunction up to 3 months after coronary ligation. Delivery of the pro-angiogenic and fibroblast-activating peptide, thymosin β4, along with GMT, resulted in further improvements in scar area and cardiac function. These findings demonstrate that cardiac fibroblasts can be reprogrammed into cardiomyocyte-like cells in their native environment for potential regenerative purposes.

Heart failure affects over 14 million people worldwide and is a leading cause of death in adults and in children. Because postnatal cardiomyocytes (CMs) have little or no regenerative capacity, therapies are limited at present. The introduction of exogenous stem-cell-derived CMs holds promise, but also challenges, including delivery, integration, rejection and cellular maturation[1–3]. Reprogramming adult fibroblasts into induced pluripotent stem cells (iPSCs) that are similar to embryonic stem cells addresses some issues[4–6], but others, including efficient directed differentiation into CMs and effective delivery, remain.

A new generation of reprogramming technology involves transdifferentiating one adult somatic cell type directly into another[7–11]. We reported direct reprogramming of fibroblasts into CM-like cells *in vitro* by expressing three transcription factors: Gata4, Mef2c and Tbx5 (GMT)[7]. As observed in reprogramming to iPSCs, the percentage of fibroblast cells fully reprogrammed to beating CMs *in vitro* was small, but far more were partially reprogrammed, much like pre-iPSCs that can become fully pluripotent with additional stimuli[12]. We posited that cardiac fibroblasts may reprogram more fully *in vivo* in their native environment, which might promote survival, maturation, and coupling with neighbouring cells. If so, the vast pool of cardiac fibroblasts in the heart could serve as an endogenous source of new CMs for regenerative therapy.

Retroviral delivery of GMT *in vivo*

We used a retroviral system to express GMT, and/or dsRed as a marker, in the hearts of 2-month-old male mice by direct intramyocardial injection. After 2 days, transverse sections of the injected area were prepared and co-stained for dsRed, α-actinin (a CM marker) and vimentin (enriched in fibroblasts). No markers are uniquely specific for cardiac fibroblasts, but fibroblasts are known to express vimentin and the surface markers Thy1 and DDR2 (ref. 13). At baseline, it was difficult to detect α-actinin- or vimentin-positive cells that also expressed dsRed, suggesting minimal viral uptake, and consistent with the observation that retroviruses only infect actively dividing cells[14].

Fibroblasts are embryologically distinct from CMs in their origin[15], and following myocardial infarction (MI) become activated, migrate to the injury site, and proliferate[16,17]. We induced cardiac injury by coronary artery ligation and injected dsRed retrovirus into the myocardium bordering the infarct zone. Whereas cells co-expressing dsRed and α-actinin were still undetectable, many vimentin-positive cells were also positive for dsRed (Supplementary Fig. 1). By fluorescence-activated cell sorting (FACS), over 4% of cells (98,238 ± 5,523) from the left ventricle of injected hearts were dsRed$^+$ Thy1$^+$ 2 days after injury, suggesting successful delivery of virus into cardiac fibroblasts and possibly other non-myocytes upon injury (Fig. 1a, b). By quantitative polymerase chain reaction (qPCR), dsRed$^+$ Thy1$^+$-sorted cells expressed about 60-fold more GMT than dsRed$^-$ Thy1$^+$ cells, and 6–8-fold more than endogenous CMs (Fig. 1c). A similar number of dsRed$^+$ Thy1$^-$ cells represented other non-myocyte cell types. Endothelial cells (PECAM$^+$) and some perivascular cells (NG2$^+$; also known as Cspg4) were also transduced by the retrovirus, but haematopoietic (CD34$^+$) and pericardial (WT1$^+$) cells were not (Supplementary Fig. 1).

Reprogramming into induced cardiomyocytes

To determine whether new cardiomyocytes could be created *in vivo* from cells other than post-mitotic CMs, we used lineage-tracing experiments to track the origin of putative induced cardiomyocytes (iCMs). To label cells genetically, we used a mouse transgenic line that expresses Cre recombinase under the promoter of the fibroblast-enriched gene, periostin[15,18,19]. When intercrossed with the R26R-lacZ reporter line[20], in which β-galactosidase is activated only in periostin-Cre-expressing cells and their progeny (Fig. 1d–f), we found β-galactosidase activity in many, but not all, cardiac fibroblasts and

[1]Gladstone Institute of Cardiovascular Disease, San Francisco, California 94158, USA. [2]Department of Pediatrics, University of California, San Francisco, California 94158, USA. [3]Department of Biochemistry and Biophysics, University of California, San Francisco, California 94158, USA. [4]Cardiovascular Research Institute, University of California, San Francisco, California 94158, USA. [5]Department of Medicine, University of California, San Francisco, California 94158, USA. [6]Developmental Biology and Neonatal Medicine Research Program, Indiana University School of Medicine, Indianapolis, Indiana 46202, USA.

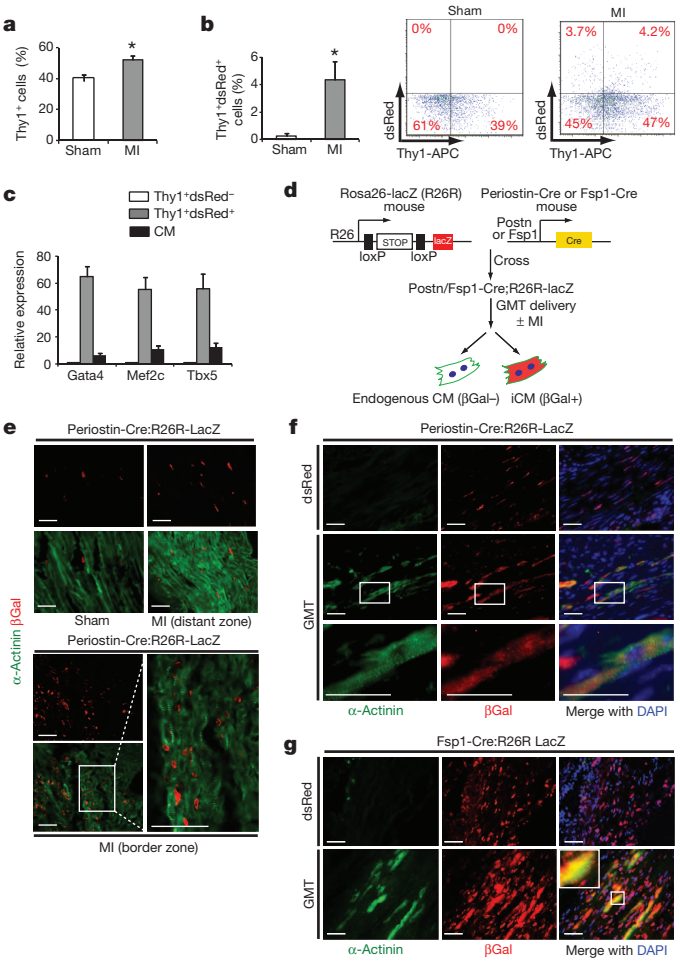

Figure 1 | Genetic lineage tracing demonstrates *in vivo* reprogramming of cardiac fibroblasts to CM-like cells. **a**, Quantification of FACS analyses for Thy1$^+$ cells from sham-operated mouse hearts or hearts 2 days after MI ($n = 3$, $^*P < 0.05$). **b**, FACS analyses of Thy1$^+$ dsRed$^+$ cells from sham-operated or post-MI hearts injected with dsRed-expressing retrovirus, with quantification (left) and representative FACS plots (right) ($n = 3$, $^*P < 0.05$). APC, allophycocyanin. **c**, qPCR analysis of Gata4, Mef2c and Tbx5 in Thy1$^+$ dsRed$^+$ cells or endogenous CMs compared to Thy1$^+$ dsRed$^-$ cells sorted 2 days after post-MI intramyocardial Gata4, Mef2c, Tbx5 and dsRed (GMTR) injection. $n = 3$ with technical quadruplicates. **d**, Schematic diagram showing the genetic fate mapping method to trace the lineage of CMs reprogrammed from periostin-Cre:R26R-lacZ or Fsp1-Cre:R26R-lacZ cells. βGal, β-galactosidase; Postn, periostin. **e**, Immunofluorescent staining for α-actinin (green) and β-galactosidase (red) on sham-operated or post-MI periostin-Cre:R26R-lacZ mouse hearts 4 weeks post-surgery. Images are from distant or border zones where endogenous CMs were labelled by α-actinin, but were never co-localized with β-galactosidase ($n = 5$ hearts per condition, 8 sections per heart). Scale bar, 50 μm. **f**, **g**, Immunofluorescent staining for α-actinin, β-galactosidase and DAPI in infarct areas of dsRed- or GMT-injected periostin-Cre:R26R-lacZ (**f**) or Fsp1-Cre:R26R-lacZ (**g**) mouse hearts 4 weeks after MI. Boxed areas indicate regions of magnification. Scale bar, 50 μm. Error bars indicate standard error of the mean (s.e.m.).

some endocardial and endothelial cells, as previously reported[15,18,19]. Periostin-Cre activity was absent in bone marrow cells (not shown). β-Galactosidase activity was not detected in any cardiomyocytes, even 4 weeks after injury, consistent with thoracic aortic banding studies, confirming that the periostin-Cre mice mark only descendants of the non-myocyte population, even after MI (Fig. 1e)[15,18,19]. Isolation of single CMs from these hearts confirmed the absence of β-galactosidase activity in over 1,500 CMs per heart from 6 mice.

In contrast, 4 weeks after MI and retroviral delivery of GMT, numerous β-galactosidase$^+$ cells were α-actinin$^+$ in the injured areas, with well-formed sarcomeres and shapes similar to β-galactosidase$^-$ myocytes, suggesting that they were descendants of cells that once expressed periostin (Fig. 1f). Similar results were obtained using transgenic mice in which Cre recombinase was under the control of the fibroblast-specific protein 1 (Fsp1; also known as S100a4) promoter[21] to label the non-myocyte population (Fig. 1g and Supplementary Fig. 2a–f). Thus, analogous to induction of cardiac fibroblasts into skeletal muscle *in vivo* upon introduction of the skeletal muscle master regulator, MyoD[22], GMT appeared to induce the formation of cardiomyocytes *in vivo*. We determined if endothelial and circulating haematopoietic cells marked by Tie2-Cre:R26R-lacZ[23] transgenic mice could be reprogrammed to express sarcomeric markers, but found no evidence for such an event (Supplementary Fig. 2g–i).

We formally tested whether retroviral introduction of GMT into non-myocytes could promote cell fusion events in the heart, thereby generating α-actinin$^+$ β-galactosidase$^+$ cells. We 'pulse-labelled' endogenous CMs in transgenic mice with Cre under inducible control of the α-MHC (also known as Myh6) promoter (α-MHC-MerCreMer)[24] crossed with R26R-EYFP mice (Supplementary Fig. 3). Subsequently, hearts were injured and infected retrovirally with GMT and dsRed to mark infected dividing cells. After 4 weeks, we detected no YFP$^+$ cells co-labelled with dsRed in the GMTdsRed- or dsRed-infected hearts (Fig. 2a, b and Supplementary Fig. 4a). Because pulse labelling marks only ~80% of endogenous CMs in the uninjured heart and ~60% in the infarct border zone[25], we quantified the percentage of YFP$^+$ pulse-labelled endogenous CMs at the border area. GMT introduction resulted in a reduced percentage of YFP$^+$ endogenous CMs compared to total CMs, indicating that the CMs in this region were refreshed by new iCMs (Fig. 2c). These findings suggest that it is unlikely that cell fusion makes a major contribution to the α-actinin$^+$ β-galactosidase$^+$ cell population, although a minor contribution cannot be ruled out.

If α-actinin$^+$ β-galactosidase$^+$ cells instead resulted from cellular reprogramming, one might detect progressive stages of reprogramming over time, as cell fusion would yield mature cells soon after fusion without intermediate stages. We therefore analysed heart sections 1, 2, 3 and 4 weeks after injury and GMT infection, and classified cells into four groups based on increasing α-actinin expression and organization into sarcomeres. The number of α-actinin$^+$ β-galactosidase$^+$ cells in the infarct area increased temporally, as did the maturity of the cells, with progressive increases in the percentage of cells with well-developed sarcomeres (Supplementary Fig. 5).

To avoid false positives from overlaying cells due to the thickness of the heart sections, we isolated adult CMs at the single-cell level from the infarct/border zone of periostin-Cre:R26R-lacZ reprogrammed hearts 4 weeks after coronary ligation (Supplementary Fig. 6a). In this preparation, non-myocytes were removed, and cells were assayed 2–4 h after primary culture. No CMs isolated from dsRed-injected hearts were β-galactosidase$^+$ by immunostaining (Fig. 2d). Similarly, CMs from periostin-Cre:R26R-EYFP mice were all YFP$^-$, among the thousands of cells visualized, in agreement with the absence of periostin-Cre activity in myocytes after injury. In contrast, 35% of cells in the CM preparation from the border/infarct zone were β-galactosidase$^+$ after GMT injection (Fig. 2e, f and Supplementary Fig. 6b). Among the β-galactosidase$^+$ cells, 98% were also α-actinin$^+$ (Supplementary Fig. 7a–d). Furthermore, in hearts co-injected with GMT and dsRed retrovirus, β-galactosidase$^+$ CMs were also positive for dsRed, indicating retroviral infection and their likely origin from non-post-mitotic CMs (Fig. 2g–k).

Most β-galactosidase$^+$ cells were large, rod-shaped and binucleated, closely resembling endogenous CMs that were β-galactosidase$^-$ from the same preparation. In addition to α-actinin, β-galactosidase$^+$ cells expressed multiple sarcomeric markers, including tropomyosin (Fig. 2m), α-MHC (Fig. 2n), and cardiac troponin T (cTnT; also known as Tnnt2) (Fig. 2o). Half of the cells had nearly normal sarcomeric structures throughout the cell. The full spectrum of reprogrammed cells, classified by quality of sarcomeric structure, is shown in

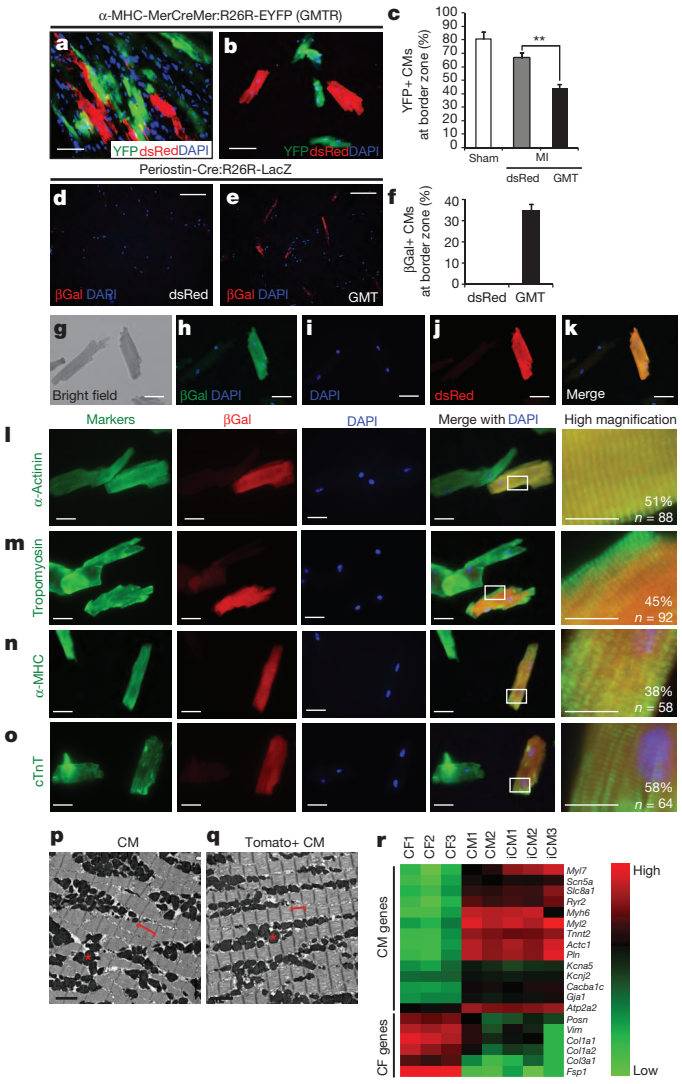

Figure 2 | Cellular analysis of the degree of *in vivo* cardiac reprogramming. **a**, Immunofluorescent staining for YFP, dsRed and DAPI on heart sections from tamoxifen pulse-labelled reprogrammed hearts injected with GMTR. Scale bar, 50 μm. **b**, Immunofluorescent staining for YFP, dsRed and DAPI on isolated CMs from the infarct/border zone of pulse-labelled reprogrammed hearts. Scale bar, 100 μm. **c**, Quantification of the percentage of YFP$^+$ cardiomyocytes in the infarct/border zone of pulse-labelled mouse hearts injected with dsRed (control) or GMT compared to sham (**$P < 0.01$, $n = 3$). **d–f**, Immunofluorescence staining for β-galactosidase (βGal) and DAPI on isolated CMs from the infarct/border zone of periostin-Cre:R26R-lacZ hearts 4 weeks after dsRed (**d**) or GMT (**e**) injection, with quantification in **f**. $n = 221$ cells from three hearts for dsRed group; $n = 182$ cells from three hearts for GMT group. Scale bar, 200 μm. **g**, Bright-field image of CMs isolated from GMTR-injected periostin-Cre:R26R-lacZ hearts 4 weeks after MI. **h**, **j**, **k**, Among these cells, a β-galactosidase-positive cell is shown (**h**) that also co-stained with dsRed (**j**, **k**). **i**, DAPI labels nuclei. Scale bar, 50 μm. **l–o**, Immunofluorescent staining for cardiac markers—including α-actinin, tropomyosin, cardiac MHC and cTnT—co-labelled with β-galactosidase and DAPI, in isolated CMs from the infarct/border zone of periostin-Cre:R26R-lacZ hearts 4 weeks after GMT injection. The images display representative reprogrammed CMs next to endogenous CMs from the same preparation. Quantification of cells with full sarcomere development is shown, with the full spectrum of marker expression, localization, and quantification shown in Supplementary Fig. 8. White boxes in the merged pictures indicate the areas for high magnification images shown in the far right panels. Scale bar, 50 μm for the first four columns, 20 μm for the last column. **p**, **q**, Electron microscopy of endogenous CMs or reprogrammed CMs, as identified by the periostin-Cre:R26R-Tomato lineage marker (Tomato$^+$ CM). Asterisk indicates mitochondria and brackets indicate sarcomeric units. Scale bar, 2 μm. **r**, Heat map of gene expression for a panel of CM- or fibroblast-enriched genes in isolated adult cardiac fibroblasts (CFs), CMs or iCMs based on lineage markers. The complete data set with statistics is provided in Supplementary Fig. 9. Error bars indicate s.e.m.

Supplementary Fig. 7. Characterization of single dsRed$^+$ YFP$^-$ cells derived from the α-MHC-Mer-Cre-Mer-YFP pulse-labelled reprogrammed hearts revealed good sarcomere formation and expression of α-actinin, cTnT and connexin 43 (Cx43; also known as Gja1), like dsRed$^-$ YFP$^+$cells (Supplementary Fig. 4b).

By electron microscopy, about half of the cells from periostin-Cre:R26R-Tomato reprogrammed hearts exhibited well-organized sarcomeres and mitochondria (Fig. 2p, q), although the sarcomeres were consistently shorter than endogenous CMs and their Z-bands more diffuse. Other Tomato$^+$ cells displayed sarcomeric organization in parts of the cell and variable mitochondria organization (Supplementary Fig. 8). For simplicity, we will refer to the β-galactosidase$^+$α-actinin$^+$ CM-like cells as *in vivo* iCMs, based on morphology and sarcomeric structure.

Finally, we assessed the reprogramming of gene expression in iCMs by qPCR, focusing on the messenger RNA levels of 20 genes normally enriched in mature CMs or cardiac fibroblasts. We tested iCMs isolated from multiple independent hearts alongside cardiac fibroblasts and endogenous CMs. mRNA levels in iCMs were similar to CMs (Fig. 2r and Supplementary Fig. 9), including the downregulation of periostin and *Fsp1*, consistent with the morphological changes described earlier.

In vivo iCMs electrically mature and couple

To determine whether iCMs expressed proteins involved in cell–cell communication similar to endogenous CMs, we examined the expression pattern of N-cadherin, a cell-surface Ca^{2+}-dependent adhesion molecule normally found in intercalated disks within the myocardium[26]. We found that over 90% of iCMs expressed N-cadherin, with 60% of cells localizing N-cadherin appropriately at the cell border (Fig. 3a). Similarly, about 90% of iCMs expressed Cx43, the major gap junction protein in the heart that promotes electrical coupling and synchronized contraction of myocytes[27]. Half of the iCMs expressed Cx43 at high levels with good localization relative to endogenous CMs (Fig. 3b), and in 4% of these cells, the Cx43 localization pattern was almost indistinguishable from endogenous CMs (Fig. 3b). Immunohistochemistry also revealed good cell-border localization of Cx43 in iCMs (Fig. 3c).

To assess the function of cell–cell junctions, we imaged the transfer of dyes—microinjected through patch pipettes—between cells, and measured the intercellular transmission of excitation, via Ca^{2+} waves, in small groups of cells isolated from the reprogrammed hearts. Cascade Blue dextran (molecular weight (MW) 10,000), which is too large to pass through gap junctions, was retained in the patched iCMs (identified by the lineage marker periostin-Cre:R26R-Tomato). In contrast, calcein (MW 600) diffused to interconnected endogenous CMs (Fig. 3d). Ca^{2+} waves propagating in an iCM or CM excited intracellular Ca^{2+} release in neighbouring cells (Fig. 3e), suggesting that iCM–CM couplings form functional syncytia (see Supplementary Movie 1).

We next performed recordings from a single-cell suspension of CMs isolated from the border/infarct zone of periostin-Cre:R26R-EYFP mice transduced with GMT, and subsequently compared the action potentials generated by iCMs (YFP$^+$) and endogenous CMs (YFP$^-$) using standard patch-clamp techniques. Approximately 50% of patched iCMs had a physiological resting membrane potential (−70 mV or less) and 50% of iCMs exhibited contractions in response to electrical stimulation, similar to adult ventricular CMs, which are normally quiescent without stimulation (Fig. 3f and Supplementary Movie 2). Electrophysiology parameters assayed were similar to endogenous ventricular CMs (Fig. 3g). In agreement, intracellular

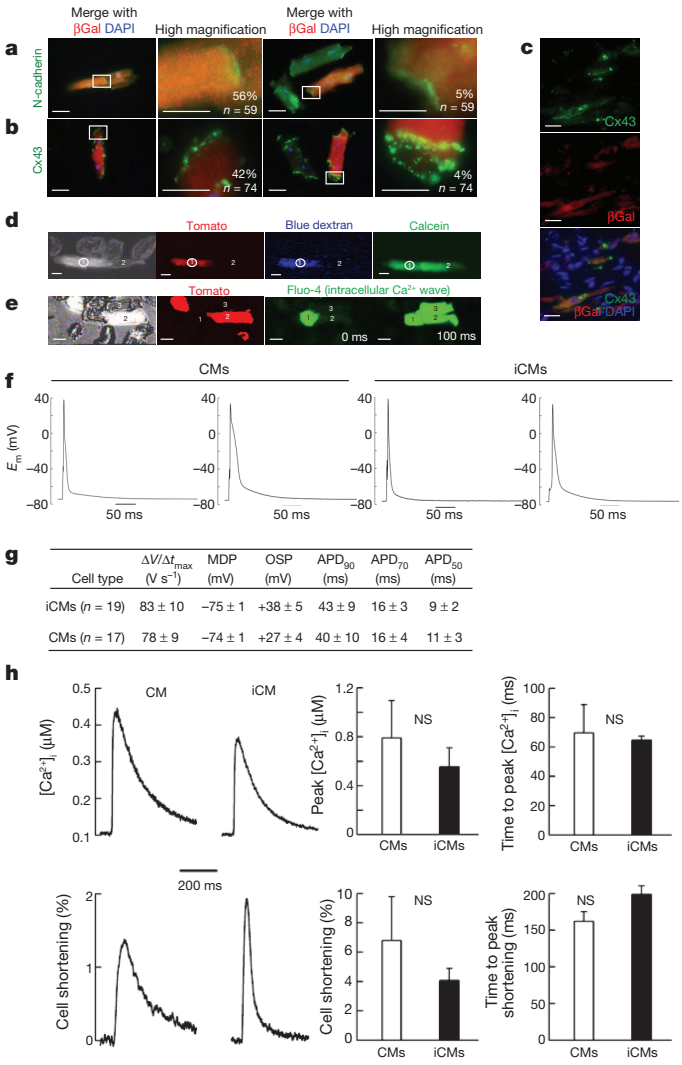

Figure 3 | Electrophysiological properties of iCMs. **a**, **b**, Immunofluorescent staining for N-cadherin (**a**) or Cx43 (**b**), co-labelled with β-galactosidase (βGal) and DAPI in isolated CMs from periostin-Cre:R26R-lacZ hearts 4 weeks after injury. Boxed areas are shown in higher magnification with the per cent of cells having the indicated morphology. Green cells represent endogenous CMs, and red/orange cells are iCMs. **c**, Immunohistochemistry for Cx43 on sections from the infarct/border zone of periostin-Cre:R26R-lacZ hearts 4 weeks after GMT injection. Scale bar, 50 μm in the first and third columns of **a** and **b**, and all of **c**; 20 μm in the second and fourth columns of **a** and **b**. **d**, Representative images of two CMs in contact with one another, including an iCM (red, cell 1) and an endogenous CM (non-red, cell 2) loaded with large (dextran) or small (calcein) dye. The large blue dextran dye loaded in the iCM (cell 1) by whole-cell patch-clamp method did not travel to the CM (cell 2), but the smaller, gap-junction-permeable dye calcein did cross the cell border ($n = 5$). Scale bar, 50 μm. **e**, Video frames captured from a group of myocytes, including endogenous CMs (non-red, cells 1 and 3) and an iCM (red, cell 2) imaged for Fluo-4 fluorescence transients corresponding to sarcoplasmic reticulum Ca^{2+} releases. Video frames 100 ms apart show that the Ca^{2+} release has spread throughout the myocyte group, including the iCM ($n = 6$). Scale bar, 50 μm. **f**, Intracellular electrical recording of *in vivo*-derived YFP^+ iCMs and endogenous YFP^- CMs from the same preparation. E_m, membrane potential in millivolts. **g**, Table of action potential parameters measured for CMs and iCMs, including maximum upstroke velocity ($\Delta V/\Delta t_{max}$) and minimum diastolic potential (MDP) measured immediately preceding stimulation, overshoot potential (OSP), and the APDs at 90, 70 and 50% repolarization. **h**, Characteristic single-field-stimulated intracellular calcium transients ($[Ca^{2+}]_i$) recorded from endogenous (left) or induced (right) CMs. Bottom, the simultaneously recorded per cent cell shortening responses triggered by the Ca^{2+} transients, in the same two cells. Quantifications from 6 iCMs and 4 endogenous CMs are shown in the right four panels. NS, not significant. For experiments performed in **d**–**h**, cells were isolated from periostin-Cre:Rosa-YFP mice 8 weeks post-MI and virus transduction. Error bars indicate s.e.m.

calcium releases and cell shortening in iCMs were comparable to endogenous CMs (Fig. 3h). The distribution of action potential durations (APDs) was bimodal in iCMs and CMs, suggesting that reprogrammed cells were incorporated near the epicardial (short APD_{90} (action potential duration at 90% of repolarization)) and endocardial (long APD_{90}) sides of ventricular tissue (Supplementary Fig. 10).

In vivo GMT improves cardiac function

Because *in vivo* reprogrammed iCMs had contractile potential and electrically coupled with viable endogenous CMs (and other iCMs), we asked whether converting endogenous non-myocytes into new myocytes translates into partial restoration of heart function after MI. All studies were performed in a blinded fashion, including the retroviral injections, and were decoded only after completion of the measurements. By Evans blue/triphenyltetrazolium chloride (TTC) double staining, the area at risk (AAR) and the infarct size were similar in GMT- or dsRed-injected mice 48 h after coronary ligation (Supplementary Fig. 11a). Three months after MI, cardiac function was examined by magnetic resonance imaging (MRI). The fraction of blood ejected with each ventricular contraction (ejection fraction), the volume of blood ejected (stroke volume), and the total cardiac output per minute were significantly improved in GMT-infected mice, particularly the stroke volume and cardiac output, possibly due to cardiac enlargement (Fig. 4a). To determine the time course of these improvements, other mice underwent serial high-resolution two-dimensional echocardiography 1 day before MI, and 3 days, 1, 4, 8 and 12 weeks after MI (Supplementary Fig.11b–d). All mice showed a comparable reduction in left ventricular function after coronary artery ligation (Supplementary Fig. 11c). Although different imaging approaches yield different absolute value norms, the overarching trends observed by echocardiography were similar to our MRI findings, in that functional improvements for all parameters were statistically significant 8 and 12 weeks after injection (Supplementary Fig. 11c).

We next performed qPCR to monitor the expression levels of atrial natriuretic factor, brain natriuretic peptide and tenascin C in injured and control hearts. We found that MI led to the upregulation of all three peptides, but this upregulation was attenuated in GMT-injected infarcted hearts (Fig. 4b). Expression levels of collagen genes, which were increased in dsRed-infected MI hearts, were also partially restored by injecting GMT (Fig. 4c). Furthermore, the scar area calculated from 16 sections at four levels of the heart was significantly smaller 8 weeks after MI in the GMT-treated group. To determine if the muscle cells in the scar area were reprogrammed iCMs, we repeated the experiments in periostin-Cre:R26R-LacZ transgenic mice. α-Actinin$^+$ cells in the scar area were also β-galactosidase positive, suggesting that they were newly born iCMs of non-myocyte origin (Fig. 4e). Vascular density was significantly increased in the border zone of reprogrammed hearts at 8 weeks (Supplementary Fig. 12). Electrocardiographic (ECG) studies (telemetry) over a 24-h period did not indicate evidence for more arrhythmias in GMT- versus dsRed-injected control mice, and no mice suffered sudden death (not shown).

Thymosin β4 enhances effects of GMT *in vivo*

We hypothesized that infecting more $Thy1^+$ cells would enhance functional improvement. Thymosin β4, a 43-amino-acid G-actin monomer-binding protein, promotes cell migration[28,29], cardiac cell survival[28,30] and activates epicardial cells to become more proliferative and yield more cardiac fibroblasts and endothelial cells[31,32]. It also improves cardiac function and decreases scar size after MI[28]. To test cardiac fibroblast migration, we used a cardiac explant migration assay[7,28]. The average time for fibroblasts to migrate from adult heart explants was 3 weeks; however, thymosin β4 treatment led to equivalent fibroblast migration within 2 weeks and within only 3 days in

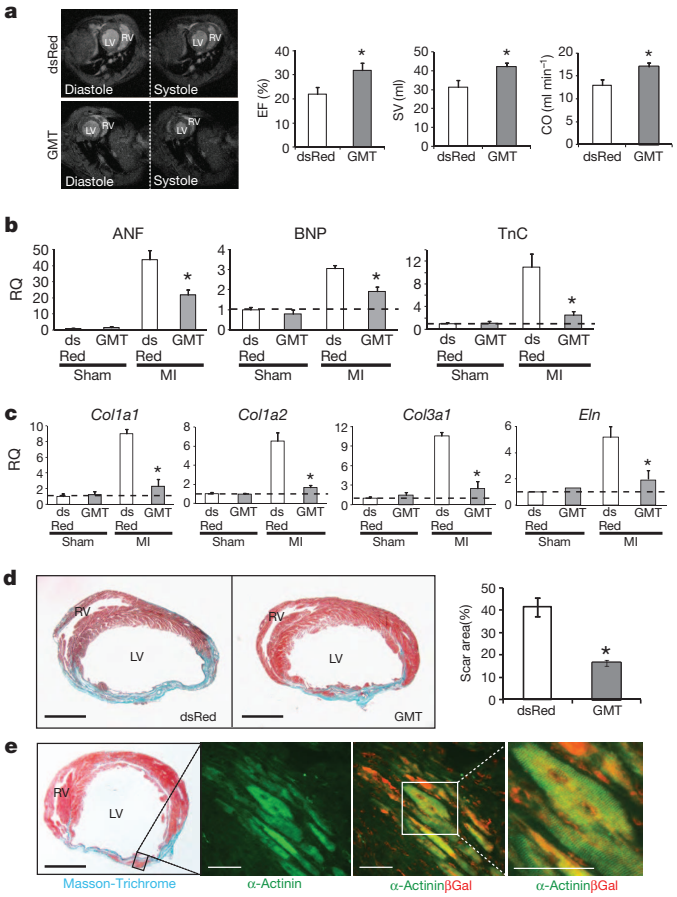

Figure 4 | *In vivo* delivery of cardiac reprogramming factors improves cardiac function after myocardial infarction. **a**, Ejection fraction (EF), stroke volume (SV) and cardiac output (CO) of the left ventricle were quantified by MRI 12 weeks after MI ($n = 9$ for each group, $^*P < 0.05$). Left four panels show representative transverse images of the thorax, containing hearts at the end of diastole (relaxation) or systole (contraction) from dsRed- or GMT-injected mice, compared to sham-operated age- and strain-matched controls. LV, left ventricle; RV, right ventricle. **b**, qPCR of atrial natriuretic factor (ANF), brain natriuretic peptide (BNP) and tenascin (TnC) on RNA extracted from the border zone of hearts 4 weeks after MI and injection of dsRed or GMT. RQ, relative quantification. **c**, qPCR of collagen type I alpha 1 (*Col1a1*), *Col1a2*, *Col3a1* and elastin (*Eln*) on RNA extracted from the border zone of hearts 4 weeks after MI and injection of dsRed or GMT. Data in **b** and **c** are relative to dsRed-injected sham-operated mice, indicated by the dashed line. $n = 3$ for each genotype with technical quadruplicates. $^*P < 0.05$. **d**, Masson-Trichrome staining on heart sections 8 weeks post-MI injected with dsRed or GMT with quantification of scar size. Scale bars, 500 μm. dsRed, $n = 8$; GMT, $n = 9$; $^*P < 0.05$. **e**, Masson-Trichrome (left) and immunofluorescent staining for α-actinin and/or β-galactosidase (βGal; right) in GMT injected periostin-Cre:R26R-lacZ mouse heart 4 weeks post-surgery. Scale bars, 500 μm in the left panel, 50 μm in the right three panels. Error bars indicate s.e.m.

heart explants taken after MI (Supplementary Fig. 13a). Similarly, vimentin$^+$ cell proliferation was even more pronounced post-MI in the presence of thymosin β4, as marked by phosphohistone H3 (Supplementary Fig. 13b). The percentage of Thy1$^+$ (Supplementary Fig. 13c) or vimentin$^+$ (Supplementary Fig. 14a) cells infected by retrovirus after MI doubled upon intramyocardial thymosin β4 injection (316,607 ± 17,799 dsRed$^+$ cells averaged from three hearts). GMT did not increase the number of cardiac fibroblasts (Supplementary Fig. 13d). Delivering GMT-expressing retrovirus to more cells by adding thymosin β4 yielded more β-galactosidase$^+$ iCMs compared to total CMs in single-cell CM culture from the infarct/border zone of periostin-Cre:R26R-lacZ hearts (51% versus 35%) (Supplementary Fig. 13e). However, we observed no change in the degree or efficiency of *in vivo* reprogramming, with the percentage of iCMs generated from the total GMT-infected cell population remaining at ~12% (Supplementary Figs 13e and 14b).

Injecting thymosin β4 immediately after ligation improved cardiac function, as previously reported[28,30]. Co-injecting thymosin β4 and GMT further improved ejection fraction and cardiac output 8 weeks after infarction (Supplementary Figs 13f and 14d, e). Furthermore, co-injecting thymosin β4 and GMT caused less scarring than injecting either alone (Supplementary Fig. 13g), despite similar areas at risk and initial infarct sizes (Supplementary Fig. 14c).

Discussion

We show that upon cardiac injury, resident cardiac non-myocytes—primarily fibroblasts—can be converted into CM-like cells *in vivo* following local delivery of GMT by retroviral-mediated gene transfer. *In vivo* cardiac reprogramming occurred with similar initial efficiency as observed *in vitro* (10–15%). However, *in vivo* iCMs were more fully reprogrammed and more closely resembled endogenous CMs than their cultured counterparts. This may result from factors within the native microenvironment—including extracellular matrix, secreted proteins, and tissue stiffness—that further enhance reprogramming. Improved cardiac function may be explained by the diversion of a small percentage of fibroblasts into new CM-like cells, suggesting functional integration of these muscle cells. Although non-myocytes convert to iCMs to help regenerate the damaged heart, alteration of fibroblast behaviour by GMT may contribute to the effects on scar formation and cardiac function. Although it is difficult to separate the relative contributions of new muscle formation and other non-cell-autonomous effects, non-myocyte reprogramming in the heart appears to be beneficial for cardiac function. Optimizing gene delivery to more cells would probably enhance functional benefits.

Improvement upon thymosin β4 addition is in agreement with the notion that increasing the delivery of GMT to more cells could enhance cardiac repair. Pre-treating hearts with thymosin β4 several days before injury resulted in a small population of epicardial-derived cells that could behave as myocyte precursors, but not if thymosin β4 was given at the time of injury[33]. Nevertheless, transduction of GMT into these progenitors, or other rare progenitors yet to be identified, might promote their differentiation into cardiomyocytes. Because thymosin β4 is also pro-angiogenic[31,32], the cooperativity between GMT and thymosin β4 may be multifaceted and will be interesting to explore.

The ability to regenerate adult heart tissue from endogenous cells is a promising approach to treating cardiac disease that may face fewer obstacles to clinical translation than other approaches. Improving the delivery of reprogramming factors, using small molecules and epigenetic modulators, and conducting trials in large animals will be important to refine the technology and assess its safety and efficacy, particularly regarding arrhythmias.

METHODS SUMMARY

Retroviruses. Retroviruses were generated as described[7] using pMXs retroviral vectors containing coding regions of Gata4, Mef2c, Tbx5 and dsRed. Ultra-high titre virus ($>1 \times 10^{10}$ plaque-forming units (p.f.u.) per ml) was obtained by ultracentrifugation.

Animals, surgery, echocardiography and electrocardiography. Periostin-Cre:R26R-lacZ or Fsp1-Cre:R26R-lacZ mice were obtained by crossing periostin-Cre mice[19] or Fsp1-Cre mice[21] and R26R-lacZ mice[20]. Periostin-Cre:R26R-EYFP or α-MHC-MerCreMer:R26R-EYFP mice were obtained by crossing periostin-Cre or α-MHC-MerCreMer[24] mice and R26R-EYFP mice. Periostin-Cre:R26R-Tomato mice were obtained by crossing periostin-Cre mice and R26R-Tomato mice. Surgeries and subsequent analyses were performed blinded to genotype and intervention. MI was induced by permanent ligation of the left anterior descending artery (LAD) as described[34]. A pool of concentrated virus (GMT or GMTR) was mixed, and 10 μl of mixed virus plus 10 μl of PBS or 40 ng μl^{-1} thymosin β4 were injected along the boundary between the infarct and border zones. Mouse echocardiography and surface electrocardiography were performed as described[34]. All mouse work was done with the approval of the University of California, San Francisco (UCSF) animal care oversight committee.

Immunohistochemistry, immunocytochemistry and electron microscopy. Immunohistochemistry, immunocytochemistry and electron microscopy were performed as described[34,35]. Scar size was determined by Masson-Trichrome staining[28,34]. The AAR and myocardial infarct size were determined by Evans blue/TTC labelling[34].

Cardiomyocyte isolation, patch-clamp, and fibroblast migration assays. Adult cardiomyocytes were isolated as described with minor modifications[36]. Single-cell patch-clamp recordings were performed as described[37]. Migration assays were performed according to published protocols[7,28].

FACS and quantitative RT–PCR. Dissociated cardiac cells were stained with APC-conjugated anti-Thy1 antibody (eBioscience). Stained cells were sorted by FACSAria2 (BD) and RNA extracted in TRizol (Invitrogen). qPCR was performed using ABI 7900HT (TaqMan, Applied Biosystems).

Statistics. Differences between groups were examined for statistical significance using unpaired Student's *t*-tests or ANOVA. $P < 0.05$ was regarded as significant.

Full Methods and any associated references are available in the online version of the paper at www.nature.com/nature.

Received 22 March 2011; accepted 14 March 2012.
Published online 18 April 2012.

1. Murry, C. E. & Keller, G. Differentiation of embryonic stem cells to clinically relevant populations: lessons from embryonic development. *Cell* **132,** 661–680 (2008).
2. Passier, R., van Laake, L. W. & Mummery, C. L. Stem-cell-based therapy and lessons from the heart. *Nature* **453,** 322–329 (2008).
3. Srivastava, D. & Ivey, K. N. Potential of stem-cell-based therapies for heart disease. *Nature* **441,** 1097–1099 (2006).
4. Takahashi, K. & Yamanaka, S. Induction of pluripotent stem cells from mouse embryonic and adult fibroblast cultures by defined factors. *Cell* **126,** 663–676 (2006).
5. Takahashi, K. *et al.* Induction of pluripotent stem cells from adult human fibroblasts by defined factors. *Cell* **131,** 861–872 (2007).
6. Yamanaka, S. & Blau, H. M. Nuclear reprogramming to a pluripotent state by three approaches. *Nature* **465,** 704–712 (2010).
7. Ieda, M. *et al.* Direct reprogramming of fibroblasts into functional cardiomyocytes by defined factors. *Cell* **142,** 375–386 (2010).
8. Szabo, E. *et al.* Direct conversion of human fibroblasts to multilineage blood progenitors. *Nature* **468,** 521–526 (2010).
9. Vierbuchen, T. *et al.* Direct conversion of fibroblasts to functional neurons by defined factors. *Nature* **463,** 1035–1041 (2010).
10. Zhou, Q., Brown, J., Kanarek, A., Rajagopal, J. & Melton, D. A. *In vivo* reprogramming of adult pancreatic exocrine cells to β-cells. *Nature* **455,** 627–632 (2008).
11. Huang, P. *et al.* Induction of functional hepatocyte-like cells from mouse fibroblasts by defined factors. *Nature* **475,** 386–389 (2011).
12. Silva, J. *et al.* Promotion of reprogramming to ground state pluripotency by signal inhibition. *PLoS Biol.* **6,** e253 (2008).
13. Ieda, M. *et al.* Cardiac fibroblasts regulate myocardial proliferation through β1 integrin signaling. *Dev. Cell* **16,** 233–244 (2009).
14. Byun, J. *et al.* Myocardial injury-induced fibroblast proliferation facilitates retroviral-mediated gene transfer to the rat heart *in vivo*. *J. Gene Med.* **2,** 2–10 (2000).
15. Snider, P. *et al.* Origin of cardiac fibroblasts and the role of periostin. *Circ. Res.* **105,** 934–947 (2009).
16. Baudino, T. A., Carver, W., Giles, W. & Borg, T. K. Cardiac fibroblasts: friend or foe? *Am. J. Physiol. Heart Circ. Physiol.* **291,** H1015–H1026 (2006).
17. Camelliti, P., Borg, T. K. & Kohl, P. Structural and functional characterisation of cardiac fibroblasts. *Cardiovasc. Res.* **65,** 40–51 (2005).
18. Snider, P. *et al.* Periostin is required for maturation and extracellular matrix stabilization of noncardiomyocyte lineages of the heart. *Circ. Res.* **102,** 752–760 (2008).
19. Takeda, N. *et al.* Cardiac fibroblasts are essential for the adaptive response of the murine heart to pressure overload. *J. Clin. Invest.* **120,** 254–265 (2010).
20. Soriano, P. Generalized lacZ expression with the ROSA26 Cre reporter strain. *Nature Genet.* **21,** 70–71 (1999).
21. Bhowmick, N. A. *et al.* TGF-β signaling in fibroblasts modulates the oncogenic potential of adjacent epithelia. *Science* **303,** 848–851 (2004).
22. Murry, C. E., Kay, M. A., Bartosek, T., Hauschka, S. D. & Schwartz, S. M. Muscle differentiation during repair of myocardial necrosis in rats via gene transfer with MyoD. *J. Clin. Invest.* **98,** 2209–2217 (1996).
23. Kisanuki, Y. Y. *et al.* Tie2-Cre transgenic mice: A new model for endothelial cell-lineage analysis *in vivo*. *Dev. Biol.* **230,** 230–242 (2001).
24. Sohal, D. S. *et al.* Temporally regulated and tissue-specific gene manipulations in the adult and embryonic heart using a tamoxifen-inducible Cre protein. *Circ. Res.* **89,** 20–25 (2001).
25. Hsieh, P. C. *et al.* Evidence from a genetic fate-mapping study that stem cells refresh adult mammalian cardiomyocytes after injury. *Nature Med.* **13,** 970–974 (2007).
26. Li, J. *et al.* Cardiac-specific loss of N-cadherin leads to alteration in connexins with conduction slowing and arrhythmogenesis. *Circ. Res.* **97,** 474–481 (2005).
27. Saffitz, J. E., Laing, J. G. & Yamada, K. A. Connexin expression and turnover: implications for cardiac excitability. *Circ. Res.* **86,** 723–728 (2000).
28. Bock-Marquette, I., Saxena, A., White, M. D., Dimaio, J. M. & Srivastava, D. Thymosin β4 activates integrin-linked kinase and promotes cardiac cell migration, survival and cardiac repair. *Nature* **432,** 466–472 (2004).
29. Goldstein, A. L., Hannappel, E. & Kleinman, H. K. Thymosin β4: actin-sequestering protein moonlights to repair injured tissues. *Trends Mol. Med.* **11,** 421–429 (2005).
30. Hinkel, R. *et al.* Thymosin β4 is an essential paracrine factor of embryonic endothelial progenitor cell-mediated cardioprotection. *Circulation* **117,** 2232–2240 (2008).
31. Smart, N. *et al.* Thymosin β4 induces adult epicardial progenitor mobilization and neovascularization. *Nature* **445,** 177–182 (2007).
32. Bock-Marquette, I. *et al.* Thymosin β4 mediated PKC activation is essential to initiate the embryonic coronary developmental program and epicardial progenitor cell activation in adult mice *in vivo*. *J. Mol. Cell. Cardiol.* **46,** 728–738 (2009).
33. Smart, N. *et al. De novo* cardiomyocytes from within the activated adult heart after injury. *Nature* **474,** 640–644 (2011).
34. Qian, L. *et al.* miR-24 inhibits apoptosis and represses Bim in mouse cardiomyocytes. *J. Exp. Med.* **208,** 549 (2011).
35. Larsen, T. H., Saetersdal, T. & Grong, K. The ultrastructure of the myocyte in different regions of experimental infarcts in the cat heart. *Res. Exp. Med. (Berl.)* **186,** 295–306 (1986).
36. Xu, H., Guo, W. & Nerbonne, J. M. Four kinetically distinct depolarization-activated K^+ currents in adult mouse ventricular myocytes. *J. Gen. Physiol.* **113,** 661–678 (1999).
37. Fenske, S. *et al.* HCN3 contributes to the ventricular action potential waveform in the murine heart. *Circ. Res.* **109,** 1015–1023 (2011).

Supplementary Information is linked to the online version of the paper at www.nature.com/nature.

Acknowledgements We are grateful for technical assistance from the Gladstone Histology Core (C. Miller), Gladstone Genomics Core (L. Ta, Y. Hao, B. Chadwick), UCSF MRI Core (M. Wendland, J. Hawkins) and Laboratory for Cell Analysis at UCSF (S. Elmes). We thank all the members of the Srivastava laboratory for helpful discussions; G. Howard and B. Taylor for editorial help; and B. Bruneau and B. Conklin for helpful discussions and critical reviews of the manuscript. We also thank J. Nerbonne, N. Foeger, and members of the Nerbonne laboratory for assistance with the adult myocyte isolation protocol. L.Q. is a postdoctoral scholar of the California Institute for Regenerative Medicine (CIRM). V.V. is supported by grants from the GlaxoSmithKline Research and Education Foundation and the NIH/NHLBI (K08HL101989). J.-d.F. is supported by a postdoctoral fellowship from American Heart Association. S.J.C. was supported by R01 HL060714 from NHLBI/NIH. D.S. was supported by grants from NHLBI/NIH, CIRM, the Younger Family Foundation, Roddenberry Foundation and the L.K. Whittier Foundation. This work was supported by NIH/NCRR grant (C06 RR018928) to the Gladstone Institutes.

Author Contributions L.Q. designed, supervised and performed the experiments. Y.H. performed all surgeries, echoes and ECGs, and contributed to tissue sectioning and sample preparation. C.I.S. performed all cellular electrophysiology experiments. A.F. quantified scar size and induced CMs and helped with mouse colony maintenance. V.V. helped with isolation of adult CMs and implantation of transmitters. S.J.C. provided periostin-Cre:Rosa26-lacZ mice and supplemental data. J.-d.F. provided initial reagents and technical knowledge and helpful discussion. D.S. designed and supervised the work. L.Q. and D.S. wrote the manuscript.

Author Information Reprints and permissions information is available at www.nature.com/reprints. The authors declare competing financial interests: details accompany the full-text HTML version of the paper at www.nature.com/nature. Readers are welcome to comment on the online version of this article at www.nature.com/nature. Correspondence and requests for materials should be addressed to D.S. (dsrivastava@gladstone.ucsf.edu).

METHODS

Retrovirus generation, concentration, and titration. Retroviruses were generated as described[7]. To generate virus, pMXs retroviral vectors containing the coding regions of Gata4, Mef2c, Tbx5 and dsRed were transfected into Plat-E cells using Fugene 6 (Roche). Forty-eight hours after transfection, virus-containing supernatants were collected and concentrated by standard ultracentrifugation. Retroviral titration was performed using the Retro-X qRT–PCR Titration Kit (Clontech), as per the manufacturer's protocols. Ultra-high titre virus ($>1\times10^{10}$ plaque-forming units (p.f.u.) per ml) was resuspended in PBS. After verification of high transduction efficiency in cell culture (>95%), a large number of small stock aliquots (10 μl) were made and frozen at −80 °C to ensure consistency among experiments. After one freeze–thaw cycle, titrations were repeated to ensure that active virus was maintained at the desired 1×10^{10} p.f.u. concentration for *in vivo* injection.

Mouse lines. Periostin (Postn)-Cre:R26R-lacZ mice were obtained by crossing Postn-Cre mice and Rosa26-lacZ mice. Postn-Cre:R26R-YFP mice were obtained by crossing Postn-Cre mice and Rosa26-EYFP mice, and Postn-Cre:R26R-Tomato mice were obtained by crossing Postn-Cre mice and Rosa26-Tomato mice. All transgenic lines for immunohistochemistry and single cell isolation were maintained by crossing with C57BL6 mice (Charles River). BALB/C mice (Charles River) were used for all functional studies after permanent ligation of the left anterior descending artery (LAD) and virus injection. Fsp1-Cre, Tie2-Cre and Myh6-MerCreMer mice were obtained from Jackson Labs, and lines were validated before further breeding. Fsp1-R26R, Tie2-R26R and Myh6-MerCreMer-YFP mice were obtained by crossing Fsp1-Cre, Tie2-Cre or Myh6-MerCreMer mice to R26R-lacZ or R26R-EYFP mice. Efficiency of Cre recombination induction for Myh6-MerCreMerYFP was tested by immunohistochemistry for YFP after injection of various doses of tamoxifen. To pulse label the pre-existing CMs, adult Myh6-MerCreMerYFP mice (8–12-weeks old) were treated with tamoxifen (Sigma) by intraperitoneal injection once a day for 5 days at a dosage of 20 mg kg^{-1} day^{-1}. GMT delivery and coronary artery ligation were performed 2 days afterwards.

Mouse MI model and *in vivo* delivery. The animal protocol for surgery was approved by institutional guidelines (UCSF Institutional Animal Care and Use Committee). All surgeries and subsequent analyses were performed blinded for genotype and intervention. Mice were anaesthetized with 2.4% isoflurane/97.6% oxygen and placed in a supine position on a heating pad (37 °C). Animals were intubated with a 19 G stump needle and ventilated with room air using a MiniVent Type 845 mouse ventilator (Hugo Sachs Elektronik-Harvard Apparatus; stroke volume, 250 μl; respiratory rate, 120 breaths per minute). MI was induced by permanent ligation of the LAD with a 7-0 prolene suture as described[28]. Sham-operated animals served as surgical controls and were subjected to the same procedures as the experimental animals with the exception that the LAD was not ligated. A pool of concentrated virus (GMT, or GMTR) was mixed, and 10 μl of mixed virus plus 10 μl of PBS or 40 ng μl^{-1} thymosin β4 was injected into the myocardium through an insulin syringe with an incorporated 29 G needle (BD). Injection with a full dosage was carried out along the boundary between the infarct zone and border zone based on the blanched infarct area after coronary artery occlusion. After injection, the chest was closed with sutures and the mouse was allowed to recover with the mouse ventilator and heating pad. All surgical procedures were performed under aseptic conditions. At 2 days and 1, 2, 4, 8 and 12 weeks after occlusion and viral delivery, the hearts were removed for perfusion fix in 4% paraformaldehyde (PFA) for preparation of paraffin sections for structural analysis and immunohistochemistry or in 0.5% PFA in 5% sucrose followed by cryostat sectioning for immunofluorescent staining. Concurrently, heart tissues within the infarct zone, border zone and non-ischaemic zone distal to the infarct zone were dissected for RNA or protein isolation.

Determination of the AAR and MI size. At 48 h after coronary ligation, the mice were anaesthetized and cannulated with tubing. Evans blue (2%, Sigma) was perfused into the aorta, thus all myocardial tissue was stained blue except the AAR. The left ventricle was isolated and cut into four ~1 mm pieces with the first cut at the ligation level. Left ventricle slices were stained in 1.5% TTC for 30 min at 37 °C, and then fixed in 4% PFA overnight at 4 °C. The area of infarction was demarcated as a white area, whereas viable myocardium was stained red. Photographs were taken from both sides of each section. The AAR and the infarct area were determined via planimetry with the computer software ImagePro (Biorad). Infarct size was calculated as the percentage of MI compared with the AAR using the described methodology[38].

Determination of scar size. Standard Masson-Trichrome staining was performed on hearts 8 weeks post-viral delivery and coronary artery ligation. To determine the scar size, we used ImagePro software to measure the scar area (blue) and healthy area (red) on transverse sections spanning four levels (50 mm between two levels, with the first level starting right below the ligation) within the left ventricle of a MI heart. From each level, we measured four slices of tissues as technical quadruplicates (for a total of 16 sections). The averaged number was used for statistics and comparison. The measurements and calculations were conducted in a blinded manner.

Mouse echocardiography. Echocardiography was performed by the Vevo 770 High-Resolution Micro-Imaging System (VisualSonics) with a 15-MHz linear array ultrasound transducer. The left ventricle was assessed in both parasternal long-axis and short-axis views at a frame rate of 120 Hz. End-systole or end-diastole was defined as the phase in which the smallest or largest area of the left ventricle, respectively, was obtained and used for ejection fraction measurement. Left ventricular end-systolic diameter and left ventricular end-diastolic diameter were measured from the left ventricular M-mode tracing with a sweep speed of 50 mm s^{-1} at the papillary muscle level for calculating the shortening fraction. B-mode was used for two-dimensional measurements of end-systolic and end-diastolic dimensions.

Mouse surface electrocardiography. Mice were anaesthetized with 1.75% isoflurane at a core temperature of 37–38 °C. Four needle electrodes (AD Instruments) were placed subcutaneously in standard limb lead configurations. For each mouse, 10–20 s of continuous signals were sampled at 10 kHz in each lead configuration with a PowerLab4/30 interface (AD Instruments). Data analysis was performed offline with electronic calipers on averaged beats (Chart5Pro v5.4.2, AD Instruments).

Mouse awake electrocardiography. To record awake electrocardiograms in six reprogrammed post-MI mice and six control post-MI mice, transmitters were surgically implanted according to the manufacturer's instructions (Data Sciences International). After a 3-day recovery period, the electrocardiogram was recorded continuously for 48 h in each mouse. Tracings were analysed off-line and were scored by a blinded investigator for the presence and frequency of arrhythmias.

MRI. MRI was performed on a Varian DirectDrive 7T small-animal scanner. Each mouse was anaesthetized by inhalation of 2% isoflurane/98% oxygen administered via an MR-compatible mobile inhalation anaesthesia system (Vet Equip). The mice were put in supine position on a homemade heating bed to keep the temperature at 37 °C. Two ECG leads were inserted into the right front and left rear leg. ECG waveforms were monitored with a small animal monitoring and gating system (SA instruments). The mouse was then placed into a homemade 1H birdcage coil with an inner diameter of 32 mm. A group of ECG- (R-wave rising edge) triggered spin echo scout images were acquired first to define the oblique plane of the short axis. Then an ECG-triggered two-dimensional gradient echo sequence with an echo time of 2.75 ms, repetition time of 200 ms and a flip angle of 45° was used to obtain nine short-axis images at 12 or 13 phases per cardiac cycle. Each scan consisted of 8–9 contiguous slices spanning the left ventricle from apex to base with 1-mm thickness, a matrix size of 128×128, a field of view of 25.6×25.6 mm, and four averages.

Isolation of adult CMs. Adult CM isolation was performed as described with minor modifications[36]. Briefly, adult mice were anaesthetized with isoflurane and mechanically ventilated. Hearts were removed and perfused retrogradely via aortic cannulation with a constant flow of 3 ml min^{-1} in a Langendorf apparatus. Hearts were perfused at 37 °C for 5 min with supplemented Wittenberg Isolation Medium (WIM) containing (in mM): 116 NaCl, 5.4 KCl, 6.7 $MgCl_2$, 12 glucose, 2 glutamine, 3.5 $NaHCO_3$, 1.5 KH_2PO_4, 1.0 NaH_2PO_4, 21 HEPES, with 1.5 nM insulin, essential vitamins (GIBCO), and essential amino acids (GIBCO) (pH 7.4), followed by digestion solution (WIM, supplemented with 0.8 mg ml^{-1} collegenase II and 10 μM $CaCl_2$) for 10 min (4 min for paired CMs that were used in cell–cell coupling experiments). Hearts were then removed from the Langendorf apparatus while intact (with tissues loosely connected). Desired areas (that is, border/infarct zone) were then micro-dissected under the microscope, followed by mechanical dissociation, triturating, and resuspension in a low-calcium solution (WIM, supplemented with 5 mg ml^{-1} BSA, 10 mM taurine, and 150 μM $CaCl_2$). Cells were then spun at low speed, supernatant was removed, and calcium was gradually reintroduced through a series of washes. For electrophysiology experiments, cells were used on the same day as isolation and until recording were stored at room temperature (21 °C) in M199 (Gibco) supplemented with 5 mM creatine, 2 mM L-carnitine, 5 mM taurine and 1.5 nM insulin. For immunohistochemistry, cells were plated onto laminin-coated culture slides, allowed to adhere, and fixed on the day of isolation. For electron microscopy or qPCR, iCMs were selected manually by micro-pipette based on the presence of periostin-Cre:R26R-YFP/Tomato signal under the fluorescent microscope right after isolation.

Cardiac fibroblast migration assay. The migration assay was performed according to the explant culture protocol as described[13]. In brief, isolated adult mouse hearts were minced into small pieces less than 1 mm^3 in size. The explants were plated on gelatin-coated dishes and cultured in explant medium (IMDM, 20% FBS) until fibroblasts migrated out from minced tissue. The time required for ten heart pieces to have migratory fibroblasts surrounding them were recorded.

FACS analyses and sorting. At 48 h after LAD and viral introduction, hearts were removed and minced into small pieces less than 1 mm^3 in size. Blood cells and debris were removed by several washings of PBS. Minced cardiac tissues were digested in an eppendorf tube and shaken with glass beads in enzyme buffer (collagenase/dispase plus DNaseI; Roche) at 37 °C. After passing through a 40-μm cell strainer, dissociated cardiac cells were stained with APC-conjugated anti-Thy1 antibody (eBioscience) for 30 min at room temperature. After washing with PBS twice, stained cells were sorted by FACSAria2 (BD).

Immunohistochemistry. For immunofluorescence, after perfusion-fixed hearts were taken out and fixed in 0.5% PFA overnight, ventricles below the ligation were embedded in OCT compound and frozen in liquid nitrogen. Sections were blocked in Universal Blocking Buffer (BioGenex) for 10 min, and then stained with primary antibodies against α-actinin (Sigma Aldrich), vimentin (Progen), β-galactosidase (Abcam), pH3 (Millipore), RFP (Biovision), Thy1 (BD), CD34 (Abcam), WT1 (Abcam), PECAM (BD), NG2 (Millipore) and GFP (Invitrogen) for 1 h at room temperature. After washing three times with PBST (PBS plus 0.1% Triton), sections were incubated in secondary antibodies for 1 h followed by washing an additional three times with PBST. Finally, the sections were mounted in Vectashield with DAPI (Vector Laboratories).

Immunocytochemistry. Isolated cells plated on chamber slides were fixed in 4% PFA at 4 °C overnight and washed with PBS twice. Cells were then incubated with primary antibodies against sarcomeric α-actinin (Sigma Aldrich), cTnT (Thermo Scientific), RFP (Biovision), tropomyocin (Hybridoma Bank), MF20 (Hybridoma Bank), Cx43 (Sigma Aldrich), N-cadherin (Invitrogen), β-galactosidase (Abcam), smooth muscle actin (Sigma Aldrich) and vimentin (Progen) for 1 h at room temperature and washed with PBS three times, then incubated with secondary IgG antibodies conjugated to Cy 488 or 594 (Jackson Immunoresearch) for 30 min. After washing with PBS, cells were mounted in Vectashield with DAPI.

Electron microscopy. For electron microscopy, cells were fixed in 2% glutaraldehyde, 1% paraformaldehyde in 0.1 M sodium cacodylate buffer, pH 7.4, post fixed in 2% osmium tetroxide in the same buffer, *en bloc* stained with 2% aqueous uranyl acetate, dehydrated in acetone, infiltrated, and embedded in LX-112 resin (Ladd Research Industries). Samples were ultrathin sectioned on a Reichert Ultracut S ultramicrotome and counter stained with 0.8% lead citrate. Grids were examined on a JEOL JEM-1230 transmission electron microscope (JEOL USA) and photographed with the Gatan Ultrascan 1000 digital camera (Gatan).

Action potential recordings. Isolated myocytes suspended in tissue culture medium were transferred to a superfusion chamber (RC-26GLP; Warner Instruments) on the stage of a Nikon TiS inverted fluorescence microscope equipped with a dual wavelength microfluorometer (IonOptix). Myocytes isolated from either periostin-Cre:R26R-YFP or periostin-Cre:R26R-Tomato hearts after GMT infection were identified as control CMs or iCMs on the basis of Tomato fluorescence (Texas red optics with exciter 560 ± 55 nm, emitter 645 ± 75 nm) or YFP (standard FITC optics), and were chosen for study if they lacked spontaneous beating and partial contractures. The myocytes were whole-cell patch-clamped using an Axopatch 200B amplifier and pClamp software (Molecular Devices). Patch electrodes of 2–5 MΩ (1B-150F; WPI) were filled with intracellular solution containing 120 mM KCl, 20 mM NaHEPES, 10 mM MgATP, 5 mM K_2EGTA (or 0.1 mM), 2 mM $MgCl_2$, and adjusted to pH 7.1 with KOH. The cells were superfused with a modified Tyrode's extracellular solution containing 137 mM NaCl, 10 mM NaHEPES, 10 mM dextrose, 5 mM KCl, 2 mM $CaCl_2$, 1 mM $MgCl_2$, adjusted to pH 7.4 with NaOH. After GΩ seal formation, whole-cell access to the myocyte was established by applying brief pressure pulses, and the amplifier was switched to current clamp mode, whereupon the cell's resting potential developed. Action potentials were stimulated at 0.33 Hz using 2 nA, 2 ms current pulses applied through the patch pipette, and were signal averaged in tens. All membrane potentials were corrected for a −5.6 mV liquid junction potential determined via pClamp software. Finally, the amplifier was switched back to voltage clamp mode to identify individual ion channel currents as required. In some experiments, the concentration of K_2EGTA in the intracellular solution was reduced to 0.1 mM to permit excitation–contraction coupling to occur, and 100 μM K5Fluo-4 (Invitrogen Corp) was added to define the presence of cytosolic Ca^{2+} transients during action potentials. Electrophysiology data were digitized at 5 kHz and low-pass filtered at 2 kHz. Analysis was performed using pClamp, Microsoft Excel, and Origin (OriginLab) software. Action potential duration was measured from the point of maximum depolarizating voltage change ($\Delta V/\Delta t_{max}$) to 50, 70 and 90% repolarization. Unless stated, experiments were performed at room temperature.

Field stimulation experiments. Isolated myocytes were loaded with Fluo-4 for 30 min at room temperature before being transferred to the superfusion chamber. The loading solution contained a 1:10 mixture of 5 mM Fluo-4 AM in dry DMSO and PowerloadTM concentrate (Invitrogen) which was diluted 100-fold into extracellular Tyrode's solution containing suspended myocytes. An additional 20 min was allowed for de-esterification before commencing recordings. Contractions and Ca^{2+} transients were evoked by applying voltage pulses at 0.33 Hz, between platinum wires placed on either side of the cell of interest and connected to a field stimulator (IonOptix, Myopacer). The pulses were of 2 ms duration and set at 150% of the threshold required to elicit twitches. Fluo-4 fluorescence transients were recorded via a standard filter set (#49011 ET, Chroma Technology) in batches of ten to enable signal averaging. Between stimuli, the fluorescence excitation light was blocked by an electromechanical shutter (CS35; Vincent Associates). Resting fluorescence was recorded after cessation of pacing, and background light was obtained after picking up and removing the cell from the field of view with a patch electrode at the end of the experiment. The Ca^{2+} transients were calibrated using the pseudo-ratio method[39], assuming an *in situ* dissociation constant of 1.1 μM for Fluo-4[40]. Contractions were optically recorded simultaneously with Ca^{2+} transients by illuminating the cell of interest in red light ($\lambda > 665$ nm) subsequently directed to a CCD camera (IonOptix Myocam). The cell length signals were converted to voltage via a video motion director (VED 205; Crescent Electronics) and contraction amplitudes from different myocytes were normalized by calculating the per cent change in cell length.

Determination of cell–cell coupling. In experiments to assess the interconnectivity between iCMs and CMs, the whole-cell patch-clamp method was used to introduce a gap-junction-permeable (that is, mobile) and an impermeable (that is, immobile) dye into the same cell of interest within a small group of apparently coupled isolated myocytes ($n = 5$ groups from 5 independent hearts). The mobile dye was calcein (5 mM), and the immobile dye was 1 mM dextran-conjugated Cascade Blue (MW 10,000). The immobile dye was chosen to be well separated spectrally, both from calcein and from tomato, which was used for labelling iCMs (Invitrogen). The dye pair was included in standard intracellular solution (containing 5 mM EGTA) and cytoplasmic loading was allowed to proceed for 2 min, after which the patch electrode was withdrawn from the patched myocyte. The sarcolemma of the cell resealed after pulling off the pipette, aided by high EGTA levels in the filling solution, thereby trapping the dyes in the cytoplasm. Blue fluorescence from the immobile indicator was excited at 365 ± 40 nm, whereas calcein fluorescence was excited at 470 ± 40 nm. Fluorescent images were recorded using IonOptix Myocam via a video frame grabber (#166VCB, Hauppage) for processing using ImageJ software.

The functionality of cell–cell junctions was investigated by imaging the intercellular transmission of Ca^{2+} waves and excitation between myocytes pre-loaded with Fluo-4 AM as detailed above for the field-stimulation studies. Superfusion with 2 μM ouabain for 5–10 min was used to induce intracellular Ca^{2+} overload accompanied by Ca^{2+} wave activity, and videomicroscopy revealed the spatio-temporal relationships of Ca^{2+} waves translocating within and between the individual cells imaged in small, adherent groups ($n = 6$ groups from 5 independent hearts).

Quantitative RT–PCR. iCMs were manually sorted based on the presence of fluorescent lineage markers. Approximately 100 iCMs were pooled for RNA isolation. Similarly, ~100 endogenous CMs isolated using the standard Langendorf apparatus (see above) and ~500 cardiac fibroblasts using the migration assay (see above) were prepared for RNA isolation. RNA was extracted by the TRizol method (Invitrogen). RT–PCR was performed using the Superscript III first-strand synthesis system (Invitrogen). qPCR was performed using the ABI 7900HT (TaqMan, Applied Biosystems) as per the manufacturer's protocols. Optimized primers from the Taqman Gene Expression Array were used.

Statistical analyses. Differences between groups were examined for statistical significance using unpaired Student's *t*-test or ANOVA. A *P*-value < 0.05 was regarded as significant. Error bars indicate standard error of the mean (s.e.m.).

38. Kurrelmeyer, K. M. *et al.* Endogenous tumor necrosis factor protects the adult cardiac myocyte against ischemic-induced apoptosis in a murine model of acute myocardial infarction. *Proc. Natl Acad. Sci. USA* **97,** 5456–5461 (2000).
39. Cheng, H., Lederer, W. J. & Cannell, M. B. Calcium sparks: elementary events underlying excitation–contraction coupling in heart muscle. *Science* **262,** 740–744 (1993).
40. Ljubojević, S. *et al. In situ* calibration of nucleoplasmic versus cytoplasmic Ca^{2+} concentration in adult cardiomyocytes. *Biophys. J.* **100,** 2356–2366 (2011).